

# CODECSLIME: Temporal Redundancy Compression of Neural Speech Codec via Dynamic Frame Rate

Hankun Wang   Yiwei Guo   Chongtian Shao   Bohan Li   Xie Chen   Kai Yu\*

X-LANCE Lab, School of Computer Science;  
MoE Key Lab of Artificial Intelligence, AI Institute,  
Shanghai Jiao Tong University, Shanghai, China;  
MoE Key Lab of Artificial Intelligence, Jiangsu Key Lab of Language Computing  
{wanghankun, kai.yu}@sjtu.edu.cn

## Abstract

Neural speech codecs have been widely used in audio compression and various downstream tasks. Current mainstream codecs are fixed-frame-rate (FFR), which allocate the same number of tokens to every equal-duration slice. However, speech is inherently non-uniform in temporal information density. As a result, many tokens are wasted on steady-state segments like long vowels and silences. To address this mismatch, we present CodecSlime, a plugin-style method for compressing temporal redundancy through supporting dynamic frame rate (DFR) on neural speech codecs for the first time. Our method is unsupervised and architecture-agnostic, combining two key innovations, SchedFR and Melt-and-Cool, for adapting inference and training, respectively. When integrated into a typical VQ-GAN codec backbone and operating at 40 Hz DFR ( $\approx 600$  bps), the reconstruction WER of CodecSlime is reduced by up 46% relative to conventional FFR baselines with the same model architecture and similar bitrates, while other metrics are also competitive. CodecSlime also enables flexible trade-offs between reconstruction quality and bitrate: a single model supports inference at multiple frame rates and consistently outperforms FFR models at the corresponding frame rates. Audio samples are available at <https://acadarmeria.github.io/codecslime/>.

## 1 Introduction

The neural speech codec technique, originating from waveform compression [1, 2], has become widely used in text-to-speech (TTS) [3], speech language models [4] and interaction models [5], due to its strong compatibility with the discrete tokenization and auto-regressive modeling paradigms of large language models (LLMs) [6, 7]. Unlike self-supervised representations [8, 9], which typically focus on specific aspects of speech or particular downstream tasks, codecs serve broader application scenarios, for they aim to reconstruct speech signals with the best possible quality at the lowest achievable frame rate and bitrate.

Recent efforts on speech codecs include improving model structure or scaling up model size [10, 11, 12, 13], decoupling global information [14, 15], and fusing more semantic information [5, 16], etc. However, existing codecs still operate at bitrates far exceeding the fundamental theoretical limits (50 bps $\sim$ 100 bps) derived from phoneme-level statistics [17] and speech’s lexical information bottleneck [18]. A fundamental limitation stems from the mismatch between mainstream fixed-frame-rate (FFR) codecs and speech’s inherently non-uniform temporal information density [19]: FFR codecs allocate equal frames to both information-rich and redundant audio segments as long as they

\*Kai Yu is the corresponding author.

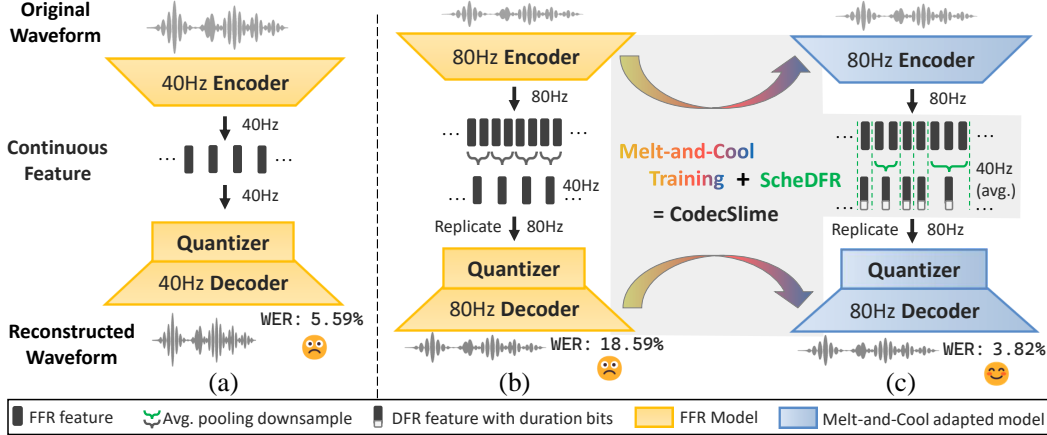


Figure 1: Comparison of : (a) conventional 40 Hz fixed-rate model, (b) 80 Hz fixed-rate model with naive fix-rate downsampling, and (c) CodecSlime-integrated model, which combines Melt-and-Cool training with ScheDFR for inference, achieving the lowest WER.

have the same time duration. Some dynamic frame rate (DFR) approaches have been attempted in previous work on discrete speech tokens, characterized by non-uniform frame durations in the encoded representation, focusing on spoken unit discovery [20] or semantics distillation [21, 22]. However, they fail to produce general-purpose acoustic tokens suitable for reconstruction and rely on overly complex training/inference procedures with limited effectiveness. Consequently, simple yet efficient methods for compressing temporal redundancy in neural codecs remain largely unexplored.

To address these issues, we introduce CodecSlime, a novel plugin-style approach that breaks the limits of traditional FFR codecs by modifying existing FFR codec backbone models for both training and inference. CodecSlime accomplishes this by introducing two core techniques: *ScheDFR* and *Melt-and-Cool*. As shown in Figure 1, *ScheDFR* adaptively merges adjacent similar frames during inference, while the *Melt-and-Cool* adapts FFR models to DFR through post-training and fine-tuning. Key advantages of CodecSlime are summarized as follows:

(1) **Enhanced performance under low frame rates and bitrates.** To reduce frame rate, the CodecSlime-integrated model first encodes speech features at a higher frame rate, then adaptively selects downsampling schemes through optimization of a feature-space distortion metric (Eq. 4), targeting maximal reconstruction quality preservation. This process inherently decouples duration and content information, enhancing information capacity over fixed-frame-rate codecs. Experimental results demonstrate CodecSlime’s effective temporal redundancy compression even under extreme conditions ( $\sim 40$  Hz average frame rate,  $\sim 600$  bps average bitrate). (2) **Frame rate controllability.** CodecSlime enables a *single model* to adapt to varying the target *average* frame rate of an utterance at inference-time. Users can flexibly trade off between frame rate and performance based on downstream requirements or resource limitations. (3) **Fully unsupervised training.** CodecSlime requires no external labels (e.g., transcripts, alignments, or speaker labels) at any training stage. This allows seamless scalability to diverse data domains. (4) **Orthogonal to codec backbones.** Though CodecSlime is implemented on a single-codebook and non-disentangled general-purpose codec backbone [10] in this work, the core *ScheDFR* and *Melt-and-Cool* techniques are backbone-agnostic and compatible with various speech tokenizer architectures

Our results demonstrate that when integrating CodecSlime with an 80 Hz FFR backbone and targeting 40 Hz during inference, the WER decreases by 46% relative to a 40 Hz FFR model with equivalent content bitrate. Even compared to an FFR model with an identical total bitrate, the WER remains 8% lower, with other metrics comparable. Furthermore, CodecSlime exhibits strong generalization: the same CodecSlime-integrated model achieves better reconstruction quality when targeting other frame rates like 50 Hz or 67 Hz compared to FFR models trained at those rates. In summary, our work represents the first systematic exploration of temporal redundancy compression in speech codecs, proposing an effective solution that opens new possibilities for future speech tokenization.

## 2 Related work

To the best of our knowledge, all neural speech codecs published so far quantize speech in an FFR manner. After the landmark EnCodec [2] and DAC [23] models, researchers have been pursuing lower bitrates along various axes, including: (1) Global redundancy reduction [14, 15] and factor disentanglement methods [24, 25, 26] that aim to implicitly or explicitly remove global information in the time-varying codes to reduce the representation space; (2) Semantic distillation [5, 27, 28, 29, 16] that incorporates self-supervised learning (SSL) features into the codec space by auxiliary guiding losses or direct fusing; (3) Model scaling and architectural refinement [10, 11, 12, 13] that aims to increase model capacity and reduce computational costs; (4) Variable-rate quantization techniques like VRVQ [30] that adapt codebook usage per frame for optimal bitrate allocation; (5) Hierarchical designs [31, 32], such as SNAC [31], that create a multi-resolution code stream to lower down the required bitrate. While these approaches reduce temporal redundancy, they remain constrained by fixed frame rates, failing to achieve adaptive dynamic compression at the frame level.

As for the broader speech tokenization field, several works address the non-uniform distribution of information in speech by varying frame rate. Dieleman et al. [19] proposed learnable temporal pooling to adaptively compress latent sequences. Variable-rate hierarchical CPC [20] introduced reinforcement learning to discover acoustic units with dynamic boundaries. Recent innovations like and SyllableLM [21] and Sylber [22] leverage syllable-aligned SSL representations to achieve ultra-low frame rates ( $\approx 5$  Hz). TASTE [33] aligns acoustic-layer tokens with the corresponding text transcription to obtain multi-layer low-frame-rate tokens.

In summary, existing methods fail to produce general-purpose acoustic tokens for reconstruction, relying on complex processes with limited effectiveness. Simple yet efficient temporal redundancy compression in codecs remains unexplored.

## 3 CodecSlime

We propose CodecSlime, a novel plugin-style method for neural codecs that enhances traditional FFR codecs by enabling DFR. It achieves flexible encoding and high-quality reconstruction at low frame rates through two key techniques: (1) Schedulable Dynamic Frame Rate (ScheDFR, § 3.2) that aggregates temporally similar features in the inference stage to enable low-loss compression; (2) Melt-and-Cool training recipe (§ 3.3), a two-stage process that adapts the FFR backbone model to better handle DFRs. The backbone model for integrating CodecSlime will be elaborated in § 3.1.

### 3.1 Backbone model

#### 3.1.1 Architecture

Our backbone model employs a VQ-GAN [34] codec architecture similar to BigCodec [10]: the generator consists of three components: an encoder, a quantizer, and a decoder, and the discriminator is made up of the MPD and MS-STFT discriminators [2, 35]. The main difference from BigCodec lies in the generator’s quantizer: we employ finite scalar quantization (FSQ) to better support DFR.

**Encoder & decoder** The encoder and decoder adopt mirrored architectures based on Convolutional Neural Networks (CNNs) and long short-term memory networks (LSTMs). Formally, let  $\mathbf{x} = \{x_1, x_2, \dots, x_W\}$  represent the input waveform and its sample points,  $f_E(\cdot)$  the encoder, and  $\mathbf{h}^{T \times d_h} = \{h_1, h_2, \dots, h_T\}$  the encoded hidden feature vector sequence. The encoding process is given by:  $\mathbf{h} = f_E(\mathbf{x})$ . The encoder contains multiple CNN blocks with a cumulative downsampling rate  $R_E$ , satisfying  $W = R_E \times T$ . After processing through CNN blocks, the features are fed into a 2-layer unidirectional LSTM to capture temporal dependencies, yielding the final encoder features  $\mathbf{h}^{T \times d_h}$ , which are then passed to the quantizer. The decoder  $f_D(\cdot)$  reconstructs the waveform  $\hat{\mathbf{x}}$  from the quantizer module’s output  $\mathbf{z}$ :  $\hat{\mathbf{x}} = f_D(\mathbf{z})$ .

**Quantizer** CodecSlime enable DFR via incorporating dynamic downsampling before quantization (§ 3.2). To better support DFR in a single codebook, we employ an FSQ quantizer [36] instead of traditional vector quantization (VQ). FSQ eliminates the need for trainable codebooks by applying a boundary transformation (typically tanh) followed by rounding to the nearest integer. Two key

advantages make FSQ particularly suitable for DFRs: (1) Low frame rates require higher information capacity per frame. FSQ trains more effectively with large codebooks (e.g., >10k entries) and achieves better codebook utilization. (2) FSQ produces smoother and more regular transitions in the quantized feature space, making downsampled features (via multi-frame averaging) easier to predict and decode. Formally, the FSQ module first projects features  $\mathbf{h}$  from  $d_h$ -dimensional space to  $d_Q$ -dimensional space, applies quantization  $f_Q(\cdot)$ , and then projects back to the original  $d_h$ -dimensional space.

**Training objective** The training loss is incorporated with reconstruction loss and GAN loss, similar to BigCodec [10]. Specifically, (1) For the reconstruction loss, we employ the multi-scale mel-spectrogram loss [23], which computes L1 distances across multiple resolution scales and demonstrates superior effectiveness compared to conventional multi-scale STFT loss [1]. (2) For the GAN loss, least-squares GAN objective and L1 feature matching loss [37] instead of binary cross-entropy loss are adopted to train the discriminator with more stability.

## 3.2 Schedulable Dynamic Frame Rate (ScheDFR)

### 3.2.1 Motivation

Speech audio can be viewed as a sequence of phonemes (and silences) where each phone is augmented with its duration and other paralinguistic information. Consequently, the information density of speech is inherently non-uniform along time. For example, while long vowels and consonants convey nearly equivalent semantic information, long vowels occupy significantly longer durations. However, in existing FFR codecs, long phonemes with less temporal variation, such as silences or sustained vowels, usually consume more frames. If a codec could automatically identify and compress temporal redundancy, it would facilitate reducing the required frame rate while improving alignment between codec tokens and phoneme sequences. To address this challenge, we propose Schedulable Dynamic Frame Rate (ScheDFR). It compresses FFR speech feature sequences to a target average frame rate while preserving reconstruction quality as much as possible.

### 3.2.2 Problem formalization

To realize ScheDFR, we insert a schedulable downsampling module between the encoder LSTM and the quantizer. It takes as input: (1) the continuous outputs  $\mathbf{h}^{T \times d_h} = f_E(\mathbf{x})$  from the encoder, and (2) the target downsampling ratio  $R_S$ . Its output is an optimal downsampling scheme  $\mathbf{s}^* = \{s_1, s_2, \dots, s_{T'}\}$  that achieves the target frame rate while maximizing reconstruction quality, where  $T' = \lceil T/R_S \rceil$ . The module contains two sequential procedures: scheduling and downsampling.

**Downsampling** Given a segment length sequence  $\mathbf{s} = (s_1, \dots, s_{T'})$  with  $\sum_{i=1}^{T'} s_i = T$ , define the starting frame index  $\sigma_1 = 1$  and  $\sigma_{i+1} = \sigma_i + s_i$ . Then, the frame-averaged downsampling function  $f_{\text{down}} : \mathbb{R}^{T \times d_h} \times \mathbb{N}^{T'} \rightarrow \mathbb{R}^{T' \times d_h}$  outputs:

$$\forall i \in [1, T'], \forall t \in [\sigma_i, \sigma_i + s_i - 1], \quad h'_t = \frac{1}{s_i} \sum_{j=\sigma_i}^{\sigma_i + s_i - 1} h_j \quad (1)$$

Note that  $\mathbf{h}'$  maintains the same temporal length  $T$  as  $\mathbf{h}$ . This process is equivalent to downsampling to  $T'$  frames, then upsampling back to  $T$  frames. Also, note that to preserve duration information losslessly, each merged frame requires additional storage of  $\log_2 U$  duration bits, which inherently decouples content and duration information.

**Scheduling** Let  $\mathcal{S} = \left\{ \mathbf{s} \mid \sum_{i=1}^{T'} s_i = T, 1 \leq s_i \leq U \right\}$ . Theoretically, the optimal scheme is obtained by:

$$\mathbf{s}^* = \arg \max_{\mathbf{s} \in \mathcal{S}} \mathcal{J}(\hat{\mathbf{x}}', \mathbf{x}) \quad \text{where } \hat{\mathbf{x}}' = f_D(f_{\text{down}}(\mathbf{h}, \mathbf{s})) = f_D(\mathbf{h}') \quad (2)$$

where  $\mathcal{J}$  denotes the reconstruction quality metric and  $U$  is the maximum allowed segment length. However, the optimization algorithm corresponding to Eq. 2 would be impractical because most reconstruction quality metrics are non-differentiable or intractable (e.g., word error rate). Enumeration is infeasible due to the prohibitively large search space, while parameterized approaches (such as reinforcement learning) also face high computational costs and unstable and complex training.

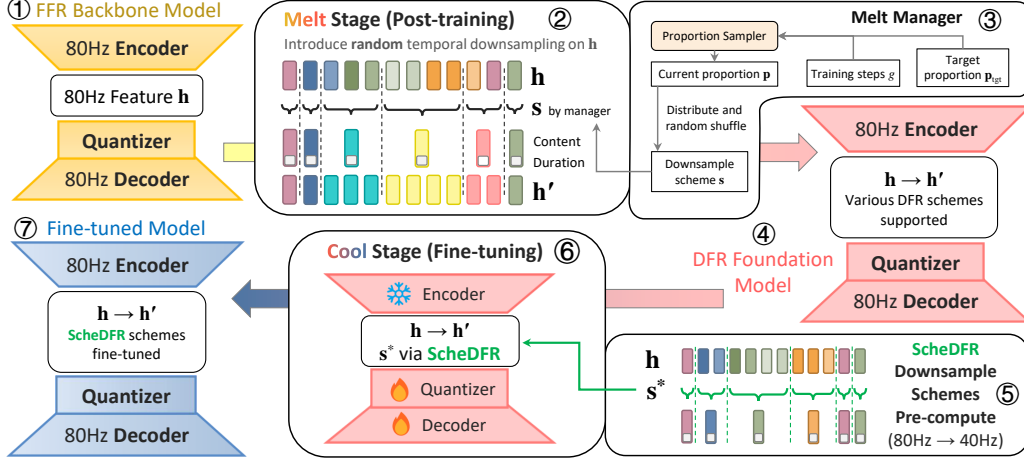


Figure 2: Overview of CodecSlime, including ScheDFR inference and Melt-and-Cool training.

**Surrogate objective** We adopt a simple feature-level surrogate metric  $\mathcal{J}_h$  that maintains strong correlation with waveform reconstruction quality (verified in § 5.3) while avoiding computational intractability.  $\mathcal{J}_h$  is used through:

$$\mathbf{s}^* = \arg \max_{\mathbf{s} \in \mathcal{S}} \mathcal{J}_h(\mathbf{h}, \mathbf{s}) \quad (3)$$

$\mathcal{J}_h$  computes pairwise feature distances within each segment:

$$\mathcal{J}_h(\mathbf{h}, \mathbf{s}) = - \sum_{i=1}^{T'} L(\sigma_i, s_i), \quad \text{where } L(j, s) = \frac{1}{s} \sum_{a=j}^{j+s-2} \sum_{b=a+1}^{j+s-1} \|h_a - h_b\|_2. \quad (4)$$

Note that segment costs are normalized by their length  $s_i$  (rather than  $\frac{s_i(s_i-1)}{2}$  pairwise combinations), which linearly scales the cost with segment length. This formulation better captures intra-segment feature cohesion compared to other objectives like L2 distance  $\sum_{j=1}^T \|h_j - h'_j\|_2$ , as it directly measures the dispersion of features within each segment. The negative sign indicates we seek segments with tightly clustered features.

We have also investigated alternative surrogate objectives, including: (1) the alignment consistency between segmentation  $\mathbf{s}$  and pre-computed phone boundaries, (2) L2 distance or cosine similarity between  $\mathbf{h}'$  and  $\mathbf{h}$ . However, experiments reveal that none of them correlate with reconstruction quality as strongly as  $\mathcal{J}_h$ . Detailed comparative experiments are presented in Appendix B.

### 3.2.3 DP-based downsample scheduler

Inspired by DPDP [38], we propose to solve the optimization of the surrogate objective  $\mathcal{J}_h$  in Eq. 3 with a dynamic-programming (DP) algorithm. Let  $d[j, i]$  denote the maximum objective value when the first  $j$  frames have been down-sampled into  $i$  frames (i.e., split into  $i$  segments). The DP runs in  $\mathcal{O}(T T' U)$  time, which maximizes  $\mathcal{J}_h$  with the DP equation below:

$$d[0, 0] = 0; \quad d[j, i] = \max_{1 \leq s \leq U} \left\{ d[j-s, i-1] - L(j, s) \right\}, \quad (5)$$

where  $L$  values can be pre-processed. The optimum is  $d[T, T']$ . The full algorithm, along with the procedures of initialization and recovering  $\mathbf{s}^*$  (via back-tracing), its efficiency analysis, and improvements, are detailed in Appendix C. Thus, through the downsample scheduler, ScheDFR adaptively identifies and compresses temporal redundancy in speech signals, achieving high-quality compression and reconstruction at low frame rates.

## 3.3 Melt-and-Cool Training Recipe

### 3.3.1 Motivation

ScheDFR achieves significant improvements over fixed-length downsampling. When applying  $2 \times$  downsampling (from 80 Hz to 40 Hz) to an FFR backbone model with a single FSQ codebook

with 18225 codes, fixed-length frame averaging yields a 45.38% WER on the test set. SchedFR ( $R_S = 2, U = 4$ ) reduces the WER by  $2.44\times$  to 18.59%, though, still remains impractical for practical deployment. This primarily occurs because the FFR backbone model lacks exposure to multi-frame downsampling scenarios during training, rendering it incapable of handling merged-frame encoding/decoding. Consequently, additional training is essential, yet no prior work addresses systematic training methodologies for a DFR codec.

To mitigate this problem, we propose a novel training recipe called Melt-and-Cool to adapt the FFR backbone model to fit downsampled features better with SchedFR enabled (Figure 2). The recipe has two stages: post-training (Melt) and fine-tuning (Cool). The circled numbers (like ①) appearing in the remainder of this section correspond to the numbered components in Figure 2.

### 3.3.2 Two-stage training

**Post-training (Melt)** This stage builds upon a well-trained FFR model (①) and trains it with a stochastic downsampling strategy (②) to obtain a DFR foundation model (④) that supports various downsampling schemes. Specifically, let the proportion of segments of each length in the total frame count  $T$  be  $\mathbf{p} = \{p_1, p_2, \dots, p_U\}$  (satisfying  $\sum_{k=1}^U p_k = 1$  and  $\sum_{k=1}^U k \cdot p_k = T$ ). Training begins with no downsampling (i.e.,  $p_1 = 1$  and  $p_{>1} = 0$ ). The downsampling schemes are controlled by the Melt manager (③): as training steps progress,  $\mathbf{p}$  gradually approaches the manually preset target proportion  $\mathbf{p}_{tgt}$ . We can easily construct and shuffle to obtain any downsample schemes  $\mathbf{s}$  that follow the specified proportion  $\mathbf{p}$  while having random segment length ordering. We also introduce randomness to the downsampling adaptation while preventing the model from deviating too much. The Melt manager’s complete algorithm is provided in Appendix A.

**Fine-tuning (Cool)** This stage fine-tunes the DFR foundation model obtained from post-training to better adapt to specific SchedFR downsampling rates and strategies. Specifically, we first use the DP-based downsample scheduler (§ 3.2.3) and the foundation model to calculate the optimal downsample scheme for each utterance in the training set under given parameters  $R_S$  and  $U$  (⑤). During fine-tuning, we no longer use random downsampling but instead use only these pre-computed optimal schemes (⑥). Meanwhile, we freeze the parameters of the foundation model encoder and only train the parameters of the quantizer and decoder (⑥). Each input still has a certain probability (30%) of bypassing downsampling to ensure model generalization and stability.

Through the above two-stage training, we successfully adapted an FFR backbone to work with SchedFR (⑦), significantly improving reconstruction quality at low frame rates.

## 4 Experimental setup

### 4.1 CodecSlime

**Backbone model** We train the backbone model using the full LibriSpeech [39] training set (960 hours of 16 kHz 16-bit audio). Model parameters include:  $R_E = 200$  (resulting in a code frequency of 80 Hz); feature dimension  $d_h = 1024$  for  $\mathbf{h}$ ; FSQ codebook size of 18225 with projected dimension  $d_Q = 8$ . All models are trained on 2 NVIDIA A800 GPUs. To better adapt to subsequent Melt-and-Cool training, the backbone model is trained using full speech utterances with dynamic batch sizes, unlike many previous works [12, 23] that crop to fixed lengths. We use AdamW [40] optimizer with moving average coefficients  $\beta_1 = 0.8$  and  $\beta_2 = 0.9$ , and a linearly decaying learning rate from  $10^{-4}$  to  $10^{-5}$  with 1000 warm-up steps. The backbone model converges in approximately 8 epochs. The training code is adopted from the official implementation of BigCodec [10].<sup>1</sup>

**Integrating CodecSlime** The main experiment of this paper is to downsample the 80 Hz backbone codec to 40 Hz. In the Melt stage, the downsample scheme generally follows a schedule where the downsampling rate gradually increases during training, with specific sampling algorithms and parameters detailed in Appendix A. The Melt stage still uses the same complete utterances and learning rate configuration as the backbone training stage. In the Cool stage, we first compute the optimal downsampling scheme for each training utterance using the DP-based downsample scheduler with  $R_S = 2, U = 4$ . During this stage, the encoder parameters are frozen, and we employ a learning

<sup>1</sup><https://github.com/Aria-K-Alethia/BigCodec>

rate decay from  $4 \times 10^{-5}$  to  $10^{-5}$ . Other settings remain the same as previous stages. Each of the two stages is trained for 2 epochs.

## 4.2 Baselines

**Official checkpoints** We compare our method with multiple state-of-the-art neural codecs: **EnCodec** [2], **DAC** [23], **LLM-Codec** [41], **SpeechTokenizer** [27], **WavTokenizer** [42], **Stable-Codec** [11], and **TS3-Codec** [12]. For EnCodec, we use the 24 kHz model operating at 1.5 kbps, where input audio is upsampled to 24 kHz before encoding and subsequently downsampled to 16 kHz for evaluation. DAC employs its 16 kHz variant, retaining only the first two codebooks to achieve a bitrate of 1 kbps. SpeechTokenizer adopts the `speechtokenizer_snake` configuration with only the first codebook retained (0.5 kbps), while Stable-Codec utilizes the checkpoint featuring the largest codebook size (729<sup>4</sup>). For WavTokenizer, the `large-320-24k-4096` model is used. LLM-Codec employs its official checkpoint. For the non-public TS3-Codec, we obtained audio samples of its X3 and X4 versions directly from the authors.

**Reproduced models** All reproduced baselines are FFR models trained using the official implementation of BigCodec [10], sharing nearly identical architecture with our backbone model except for frame rate and quantizer settings. We include three key 40 Hz variants. **BigCodec-VQ<sub>18k</sub>** uses the original VQ from BigCodec with a codebook size of 18225, matching the size of our backbone model. **BigCodec-FSQ<sub>18k</sub>** uses FSQ with 18225 codes, resulting in a model nearly identical to our backbone model except for the frame rate. **BigCodec-FSQ<sub>84k</sub>** enlarges the codebook to 84375 to match the total bitrate (content plus duration) of our CodecSlime-integrated model.

## 4.3 Testset

This paper uses three test sets: **UniCATS testset B** [43], the complete **LibriSpeech test-clean** [39], and a subset of **Multilingual LibriSpeech (MLS)** [44]. Most evaluations are conducted on UniCATS testset B, which contains 500 utterances from 37 speakers and is a subset of LibriTTS [45] test-clean. Comparisons with TS3-Codec are performed on LibriSpeech test-clean, consisting of 2620 utterances from 40 speakers. Additionally, we randomly select a 210-utterance subset (7 Western languages, 30 utterances per language) from MLS for multilingual generalization testing. All test samples are in 16-bit PCM format at 16 kHz sampling rate.

## 4.4 Metrics

**Token properties** We analyze token properties through three metrics: **frame rate**, **codebook size**, and **bitrate** (decoupled into *content* and *duration* components). The *content* bitrate is for representing acoustic features, and the *duration* bitrate is unique to our CodecSlime-integrated codec, preserving the original frame count for the downsampled tokens.

**Signal-level reconstruction quality** We evaluate short-time objective intelligibility (STOI) and Mel-cepstral distortion (MCD) as non-parameterized signal-level reconstruction metrics. MCD computes the difference of Mel cepstral coefficients, while STOI adopts a signal processing approach to mimic the human auditory system. We compute 25-dimensional MCD, and use open-sourced projects<sup>2</sup> for both metrics.

**Perceptual-level reconstruction quality** The parameterized perceptual-level reconstruction quality of speech codecs is also crucial. This includes intelligibility measured by word error rate (WER), speaker similarity measured by speaker embedding cosine similarity (SECS), and also subjective mean opinion scores. We emphasize the importance of WER scores under very low-bitrate scenarios, since the spoken content should be as unchanged as possible after codec lossy compression. In this study, we use NeMo ASR<sup>3</sup> for WER comparisons on UniCATS testset B and LibriSpeech test-clean subsets. For the MLS test set, we use Whisper-medium [46] as the ASR model. We measure the

<sup>2</sup><https://github.com/mpariente/pystoi>, <https://github.com/AI-Unicamp/TTS-Objective-Metrics>

<sup>3</sup>[https://huggingface.co/nvidia/stt\\_en\\_fastconformer\\_transducer\\_large](https://huggingface.co/nvidia/stt_en_fastconformer_transducer_large)

Table 1: Evaluation results on UniCATS testset B and LibriSpeech test-clean across all baselines listed in § 4.2. Frame Rate (Hz): Single-layer (f×1), multi-layer with identical frequencies (f×n), or different frequencies (f1+f2+...). All models operate at fixed frame rates except CodecSlime, which adapts dynamically at inference time.

Model	Frame Rate (Hz)	Codebook Size	Bitrate (kbps)		WER (%)↓	STOI↑	SECS↑	MCD↓	UTMOS↑
			Content	Duration					
Testset: UniCATS testset B [43]									
Ground Truth	-	-	256	-	1.16	1.000	1.000	0.00	4.14±0.024
EnCodec [2]	75 × 2	1024	1.50	-	4.13	0.856	0.894	2.36	1.64±0.032
DAC-1k [23]	50 × 2	1024	1.00	-	10.82	0.753	0.763	2.78	1.32±0.010
LLM-Codec [41]	8+17+33	≈32000	0.85	-	6.25	0.879	0.917	2.23	2.71±0.036
SpeechTokenizer-0.5k [27]	50 × 1	1024	0.50	-	5.01	0.642	0.581	4.57	1.25±0.001
WavTokenizer [42]	75 × 1	8192	0.98	-	5.44	0.898	0.905	2.81	3.93±0.030
Stable-Codec [11]	25 × 4	729	0.95	-	5.03	0.917	0.891	2.81	4.10±0.021
BigCodec-VQ <sub>18k</sub> [10]	40 × 1	18225	0.57	-	4.64	0.899	<b>0.932</b>	1.81	<b>4.02</b> ±0.028
BigCodec-FSQ <sub>18k</sub>	40 × 1	18225	0.57	-	5.59	0.891	0.913	1.85	3.93±0.031
BigCodec-FSQ <sub>84k</sub>	40 × 1	84375	0.65	-	4.12	0.900	0.918	<b>1.76</b>	3.99±0.028
CodecSlime	40 × 1	18225	0.57	0.08	<b>3.82</b>	<b>0.900</b>	0.916	1.83	3.93±0.029
Testset: LibriSpeech test-clean [39]									
Ground Truth	-	-	256	-	1.67	1.000	0.953	0.00	4.07±0.012
TS3-Codec (X3) [12]	40 × 1	65536	0.64	-	4.01	0.893	0.924	1.72	3.68±0.016
TS3-Codec (X4) [12]	40 × 1	131072	0.68	-	3.84	0.897	<b>0.927</b>	1.70	3.72±0.016
CodecSlime	40 × 1	18225	0.57	0.08	<b>3.84</b>	<b>0.899</b>	0.913	<b>1.65</b>	<b>3.99</b> ±0.013

SECS values of reconstructed and original speech by Resemblyzer<sup>4</sup>. We use UTMOS [47] as a proxy for the overall perceptual quality of reconstructed speech.

## 5 Results

### 5.1 Main results

Table 1 shows the comparison among baselines at approximately 40 Hz or 600 bps. CodecSlime, implemented as a 2× dynamic downsampling plugin atop BigCodec-FSQ<sub>18k</sub> 80 Hz backbone, achieves the best WER across all baselines listed. On the UniCATS testset B, it delivers the lowest WER of 3.82%, representing a 46% reduction compared to the BigCodec-FSQ<sub>18k</sub> 40 Hz FFR model (5.59%) with the same backbone and actual frame rate, while maintaining better or comparable performance on other metrics. When compared to the BigCodec-FSQ<sub>84k</sub> FFR model using the same total bitrate as CodecSlime’s content bitrate, CodecSlime’s WER is still lower with minimal degradation on other metrics, demonstrating strong semantic preservation and intelligibility reconstruction capabilities. Furthermore, CodecSlime enables a 0.6 kbps codec model to outperform 1 kbps-level baselines like Stable-Codec and EnCodec in most metrics. This fully demonstrates the effectiveness of CodecSlime in temporal redundancy compression.

On the LibriSpeech test-clean set, CodecSlime achieves superior or comparable performance across all metrics compared to the recent state-of-the-art TS3-Codec while using a lower content bitrate. Notably, CodecSlime’s UTMOS score (3.99) is very close to the Ground Truth (4.07), showcasing its exceptional perceptual quality restoration capability.

### 5.2 Evaluation of generalization ability

**On different inference frame rates** Figure 3 illustrates how WER and STOI vary across different frame rates for CodecSlime and the fixed-rate FFR baseline. In this experiment, CodecSlime uses *the same model* fine-tuned under 40 Hz ScheDFR, while the FFR baselines are separately trained models at each specific frame rate (40 Hz, 50 Hz, 67 Hz and 80 Hz). All models use FSQ with 18225 codes. The figure reveals a consistent trend: as the inference frame rate increases, WER decreases and STOI increases for both CodecSlime and FFR models. CodecSlime consistently outperforms

<sup>4</sup><https://github.com/resemble-ai/Resemblyzer>

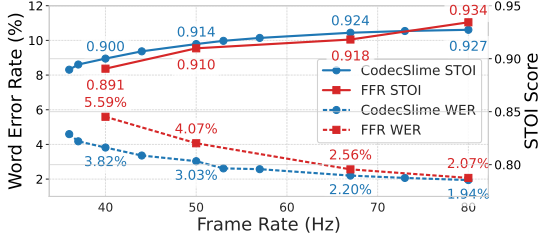


Figure 3: WER and STOI across frame rates for CodecSlime (one single model) and FFR baselines (different models for different frame rates).

Table 2: Results on the unseen languages (MLS [44]) testset.

Model	WER(%)↓	STOI↑	SECS↑	UTMOS↑
Ground Truth	8.70	1.000	1.000	2.80±0.069
BigCodec-VQ <sub>18k</sub>	37.21	0.866	0.942	2.70±0.059
BigCodec-FSQ <sub>18k</sub>	36.31	0.864	0.928	2.76±0.057
BigCodec-FSQ <sub>84k</sub>	31.28	0.876	<b>0.943</b>	<b>2.78±0.059</b>
CodecSlime	<b>30.19</b>	<b>0.877</b>	<b>0.943</b>	2.77±0.061

Table 3: Ablation results of enabling ScheDFR

Model	WER(%)↓	STOI↑	SECS↑	MCD↓
DFR Fdn. Model	5.11	0.891	0.899	1.86
+ ScheDFR	<b>4.24</b>	<b>0.898</b>	<b>0.910</b>	<b>1.83</b>
Fine-tuned Model	5.73	0.878	0.900	1.96
+ ScheDFR	<b>3.82</b>	<b>0.900</b>	<b>0.916</b>	<b>1.83</b>

Table 4: Ablation results of Melt-and-Cool

Model	WER(%)↓	STOI↑	SECS↑	MCD↓
FFR Backbone Model	18.59	0.761	0.860	2.81
+ Cool (w/o Melt)	9.53	0.844	0.904	2.13
+ Melt-and-Cool	<b>3.82</b>	<b>0.900</b>	<b>0.916</b>	<b>1.83</b>

FFR across the range from 40 Hz to 80 Hz. These results demonstrate that CodecSlime generalizes effectively across a wide range of frame rates, despite being trained only once at a single dynamic average frame rate. In contrast, FFR requires retraining separate models for each target frame rate, yet still fails to match CodecSlime’s performance. This confirms the strong generalization and flexibility of CodecSlime during inference.

**On unseen languages** We further examine the generalization ability of CodecSlime on unseen languages using the MLS test set [44]. As reported in Table 2, CodecSlime achieves a WER of 30.19, which is lower than that of all fixed-rate baselines, including BigCodec-VQ<sub>18k</sub> and BigCodec-FSQ<sub>84k</sub>. It also preserves intelligibility and perceptual quality, as reflected by competitive STOI and SECS scores (0.877 and 0.943, respectively). These results indicate that CodecSlime is able to generalize beyond its training domain and perform well in multilingual scenarios, despite being trained without supervision or language-specific priors.

### 5.3 Ablation studies

**On ScheDFR** As shown in Table 3, all 4 rows show reconstruction results from 80 Hz features downsampled to 40 Hz at inference time. Rows 1 and 3 use a fixed pattern (merging every two adjacent frames) with the DFR foundation model (backbone + Melt) and fine-tuned model (backbone + Melt + Cool), respectively. Rows 2 and 4 employ ScheDFR for dynamic downsampling with these same models. It shows that both models perform better in all metrics after equipping with ScheDFR.

**On Melt-and-Cool** In Table 4, ScheDFR is applied in all tests to downsample features from 80 Hz to 40 Hz. The 2nd row introduces only the Cool stage, which performs fine-tuning using optimal downsample schemes of the backbone model with an additional progressive training strategy incorporated that gradually increases the probability of applying downsampling at the utterance level, starting from no downsampling. Although introducing only the Cool stage brings some improvement (reducing WER from 18.59% to 9.53%), it still falls far short of the overall effectiveness achieved by the full Melt-and-Cool process (WER 3.82%). This demonstrates the effectiveness of gradually exposing the FFR model to DFR through our two-stage training recipe.

**Limitations** While surrogate objectives plus DP offer an effective solution, model-based approaches like reinforcement learning may enable better dynamic downsampling decisions. Since these approaches may lead to more concerns on training costs, generalization ability, and inference efficiency, we leave them for future work.

## 6 Conclusion

We presented CodecSlime, a plugin-style method that endows FFR neural speech codecs with DFR control. It combines an inference-time technique, ScheDFR, that merges frames via dynamic programming, and a post-training recipe, Melt-and-Cool, that acclimates the backbone to non-uniform timing. Both are fully unsupervised and architecture-agnostic. Integrated with a typical VQ-GAN backbone and inferred at 40 Hz, CodecSlime yields substantially lower WER (up to 46% relatively) than fixed-rate models of equal bitrate, while a single checkpoint generalizes across higher frame rates without retraining. These findings provide the first systematic evidence that temporal redundancy in neural codecs can be compressed effectively through DFR integration, charting a path toward more efficient speech tokenization.

## References

- [1] N. Zeghidour, A. Luebs, A. Omran *et al.*, “SoundStream: An End-to-End Neural Audio Codec,” *IEEE/ACM Trans. ASLP*, vol. 30, pp. 495–507, 2021.
- [2] A. Défossez, J. Copet, G. Synnaeve *et al.*, “High Fidelity Neural Audio Compression,” *TMLR*, 2023.
- [3] S. Chen, C. Wang, Y. Wu *et al.*, “Neural Codec Language Models are Zero-Shot Text to Speech Synthesizers,” *IEEE/ACM Trans. ASLP*, pp. 1–15, 2025.
- [4] Z. Borsos, R. Marinier, D. Vincent *et al.*, “AudioLM: A Language Modeling Approach to Audio Generation,” *IEEE/ACM Trans. ASLP*, vol. 31, pp. 2523–2533, 2023.
- [5] A. Défossez, L. Mazaré, M. Orsini *et al.*, “Moshi: A Speech-Text Foundation Model for Real-Time Dialogue,” *arXiv preprint arXiv:2410.00037*, 2024.
- [6] T. Brown, B. Mann, N. Ryder, M. Subbiah, J. D. Kaplan, P. Dhariwal, A. Neelakantan, P. Shyam, G. Sastry, A. Askell *et al.*, “Language models are few-shot learners,” *Advances in neural information processing systems*, vol. 33, pp. 1877–1901, 2020.
- [7] Y. Guo, Z. Li, H. Wang, B. Li, C. Shao, H. Zhang, C. Du, X. Chen, S. Liu, and K. Yu, “Recent advances in discrete speech tokens: A review,” *arXiv preprint arXiv:2502.06490*, 2025.
- [8] W.-N. Hsu, B. Bolte, Y.-H. H. Tsai *et al.*, “HuBERT: Self-Supervised Speech Representation Learning by Masked Prediction of Hidden Units,” *IEEE/ACM Trans. ASLP*, vol. 29, pp. 3451–3460, 2021.
- [9] V. S. Lodagala, S. Ghosh, and S. Umesh, “CCC-wav2vec 2.0: Clustering aided Cross Contrastive Self-Supervised Learning of Speech Representations,” in *Proc. IEEE SLT*, 2023, pp. 1–8.
- [10] D. Xin, X. Tan, S. Takamichi *et al.*, “BigCodec: Pushing the Limits of Low-Bitrate Neural Speech Codec,” *arXiv preprint arXiv:2409.05377*, 2024.
- [11] J. D. Parker, A. Smirnov, J. Pons *et al.*, “Scaling Transformers for Low-Bitrate High-Quality Speech Coding,” in *Proc. ICLR*, 2025.
- [12] H. Wu, N. Kanda, S. E. Eskimez *et al.*, “TS3-Codec: Transformer-Based Simple Streaming Single Codec,” *arXiv preprint arXiv:2411.18803*, 2024.
- [13] L. Della Libera, F. Paissan, C. Subakan, and M. Ravanelli, “Focalcodec: Low-bitrate speech coding via focal modulation networks,” *arXiv preprint arXiv:2502.04465*, 2025.
- [14] Y. Ren, T. Wang, J. Yi *et al.*, “Fewer-Token Neural Speech Codec with Time-Invariant Codes,” in *Proc. IEEE ICASSP*, 2024, pp. 12 737–12 741.
- [15] X. Wang, M. Jiang, Z. Ma, Z. Zhang, S. Liu, L. Li, Z. Liang, Q. Zheng, R. Wang, X. Feng *et al.*, “Spark-tts: An efficient llm-based text-to-speech model with single-stream decoupled speech tokens,” *arXiv preprint arXiv:2503.01710*, 2025.
- [16] Z. Ye, X. Zhu, C.-M. Chan *et al.*, “Llasa: Scaling Train-Time and Inference-Time Compute for Llama-based Speech Synthesis,” *arXiv preprint arXiv:2502.04128*, 2025.
- [17] P. B. Denes, “On the statistics of spoken english,” *The Journal of the Acoustical Society of America*, vol. 35, no. 6, pp. 892–904, 1963.
- [18] S. Van Kuyk, W. B. Kleijn, and R. C. Hendriks, “On the information rate of speech communication,” in *Proc. IEEE ICASSP*. IEEE, 2017, pp. 5625–5629.

- [19] S. Dieleman, C. Nash, J. Engel *et al.*, “Variable-Rate Discrete Representation Learning,” *arXiv preprint arXiv:2103.06089*, 2021.
- [20] S. Cuervo, A. Lancucki, R. Marxer *et al.*, “Variable-Rate Hierarchical CPC Leads to Acoustic Unit Discovery in Speech,” *Proc. NeurIPS*, vol. 35, pp. 34 995–35 006, 2022.
- [21] A. Baade, P. Peng, and D. Harwath, “SyllableLM: Learning Coarse Semantic Units for Speech Language Models,” in *Proc. ICLR*, 2025.
- [22] C. J. Cho, N. Lee, A. Gupta *et al.*, “Sylber: Syllabic Embedding Representation of Speech from Raw Audio,” in *Proc. ICLR*, 2025.
- [23] R. Kumar, P. Seetharaman, A. Luebs *et al.*, “High-Fidelity Audio Compression with Improved RVQGAN,” *Proc. NeurIPS*, vol. 36, 2024.
- [24] Z. Ju, Y. Wang, K. Shen *et al.*, “NaturalSpeech 3: Zero-Shot Speech Synthesis with Factorized Codec and Diffusion Models,” in *Proc. ICML*, 2024.
- [25] Y. Guo, Z. Li, C. Du *et al.*, “LSCoDec: Low-Bitrate and Speaker-Decoupled Discrete Speech Codec,” *arXiv preprint arXiv:2410.15764*, 2024.
- [26] C. J. Cho, A. Mohamed, S.-W. Li *et al.*, “SD-HuBERT: Sentence-Level Self-Distillation Induces Syllabic Organization in HuBERT,” in *Proc. IEEE ICASSP*, 2024, pp. 12 076–12 080.
- [27] X. Zhang, D. Zhang, S. Li *et al.*, “SpeechTokenizer: Unified Speech Tokenizer for Speech Language Models,” in *Proc. ICLR*, 2024.
- [28] D. Yang, J. Tian, X. Tan *et al.*, “UniAudio: Towards Universal Audio Generation with Large Language Models,” in *Proc. ICML*, 2024.
- [29] H. Liu, X. Xu, Y. Yuan *et al.*, “SemantiCodec: An Ultra Low Bitrate Semantic Audio Codec for General Sound,” *IEEE JSTSP*, pp. 1–14, 2024.
- [30] Y. Chae, W. Choi, Y. Takida *et al.*, “Variable Bitrate Residual Vector Quantization for Audio Coding,” *arXiv preprint arXiv:2410.06016*, 2024.
- [31] H. Siuzdak, F. Grötschla, and L. A. Lanzendörfer, “SNAC: Multi-Scale Neural Audio Codec,” *arXiv preprint arXiv:2410.14411*, 2024.
- [32] H. Guo, F. Xie, D. Yang *et al.*, “Speaking from Coarse to Fine: Improving Neural Codec Language Model via Multi-Scale Speech Coding and Generation,” *arXiv preprint arXiv:2409.11630*, 2024.
- [33] L.-H. Tseng, Y.-C. Chen, K.-Y. Lee, D.-S. Shiu, and H.-y. Lee, “Taste: Text-aligned speech tokenization and embedding for spoken language modeling,” *arXiv preprint arXiv:2504.07053*, 2025.
- [34] P. Esser, R. Rombach, and B. Ommer, “Taming Transformers for High-Resolution Image Synthesis,” in *Proc. IEEE/CVF ICCV*, 2021, pp. 12 873–12 883.
- [35] J. Kong, J. Kim, and J. Bae, “Hifi-GAN: Generative Adversarial Networks for Efficient and High Fidelity Speech Synthesis,” *Proc. NeurIPS*, vol. 33, pp. 17 022–17 033, 2020.
- [36] F. Mentzer, D. Minnen, E. Agustsson *et al.*, “Finite Scalar Quantization: VQ-VAE Made Simple,” in *Proc. ICLR*, 2024.
- [37] X. Mao, Q. Li, H. Xie, R. Y. Lau, Z. Wang, and S. Paul Smolley, “Least squares generative adversarial networks,” in *Proceedings of the IEEE international conference on computer vision*, 2017, pp. 2794–2802.
- [38] H. Kamper, “Word segmentation on discovered phone units with dynamic programming and self-supervised scoring,” *IEEE/ACM Trans. ASLP*, vol. 31, pp. 684–694, 2022.
- [39] V. Panayotov, G. Chen, D. Povey, and S. Khudanpur, “Librispeech: an asr corpus based on public domain audio books,” in *Proc. IEEE ICASSP*. IEEE, 2015, pp. 5206–5210.
- [40] I. Loshchilov and F. Hutter, “Decoupled weight decay regularization,” *arXiv preprint arXiv:1711.05101*, 2017.
- [41] D. Yang, H. Guo, Y. Wang *et al.*, “UniAudio 1.5: Large Language Model-Driven Audio Codec is A Few-Shot Audio Task Learner,” in *Proc. NeurIPS*, 2024.
- [42] S. Ji, Z. Jiang, W. Wang *et al.*, “WavTokenizer: an Efficient Acoustic Discrete Codec Tokenizer for Audio Language Modeling,” in *Proc. ICLR*, 2025.

- [43] C. Du, Y. Guo, F. Shen *et al.*, “UniCATS: A Unified Context-Aware Text-to-Speech Framework with Contextual VQ-Diffusion and Vocoding,” in *Proc. AAAI*, vol. 38, no. 16, 2024, pp. 17 924–17 932.
- [44] V. Pratap, Q. Xu, A. Sriram *et al.*, “MLS: A Large-Scale Multilingual Dataset for Speech Research,” in *Proc. ISCA Interspeech*, 2020, pp. 2757–2761.
- [45] H. Zen, V. Dang, R. Clark *et al.*, “LibriTTS: A Corpus Derived from LibriSpeech for Text-to-Speech,” in *Proc. ISCA Interspeech*, 2019, pp. 1526–1530.
- [46] A. Radford, J. W. Kim, T. Xu *et al.*, “Robust Speech Recognition via Large-Scale Weak Supervision,” in *Proc. ICML*. PMLR, 2023, pp. 28 492–28 518.
- [47] T. Saeki, D. Xin, W. Nakata, T. Koriyama, S. Takamichi, and H. Saruwatari, “UTMOS: UTokyo-SaruLab System for VoiceMOS Challenge 2022,” in *Interspeech 2022*, 2022, pp. 4521–4525.
- [48] D. Povey, A. Ghoshal, G. Boulianne, L. Burget, O. Glembek *et al.*, “The kaldi speech recognition toolkit,” in *Proc. IEEE ASRU*, 2011.
- [49] M.-W. Benabderrahmane, L.-N. Pouchet, A. Cohen, and C. Bastoul, “The polyhedral model is more widely applicable than you think,” in *International Conference on Compiler Construction*. Springer, 2010, pp. 283–303.

## A Details of the Melt manager

To further enhance the model’s adaptability to diverse downsampling rates and schemes, we sample from a constructed Dirichlet distribution, enabling  $\mathbf{p}$  to evolve from “easy to hard” scenarios while maintaining randomness. After reaching the preset distribution  $\mathbf{p}_{\text{tgt}}$ , the concentration of the Dirichlet distribution is slowly reduced. Additionally, we set a certain probability (typically 50%) for the input utterance to undergo no downsampling, ensuring the model’s capability does not deviate excessively. The detailed algorithm is shown in Algorithm 1.

---

### Algorithm 1: Random-proportion downsampling sample process of the Melt manager

---

**Input:** training step  $g$ , max rate  $U$ , target steps  $S_p$ , target mix  $\mathbf{p}_{\text{tgt}} \in \mathbb{R}^U$ , skip prob.  $\rho$ , auxiliary parameter for concentration control  $c$ , small constant  $\varepsilon$

**Output:** Segment lengths proportions  $\mathbf{p}$  or NONE

```

1  $u \leftarrow \text{Uniform}(0, 1)$ 
2 if  $u < \rho$  then
3   return NONE
4  $\pi \leftarrow \min(g/S_p, 1)$ 
5  $\mathbf{d} \leftarrow \pi \mathbf{p}_{\text{tgt}}$ 
6  $d_U \leftarrow 1 - \sum_{i=1}^{U-1} d_i$ 
7  $\mathbf{d} \leftarrow \max(\mathbf{d}, \varepsilon)$ 
8  $\alpha \leftarrow \mathbf{d} c / (\max(1, g/S_p))^{2.5}$ 
9  $\mathbf{p} \leftarrow \text{Dirichlet}(\alpha)$ 
10 return  $\mathbf{p}$ ;

```

---

**Symbol legend**  $g$  is the current training step.  $S_p$  denotes the number of steps required to reach the target proportion  $\mathbf{p}_{\text{tgt}}$ .  $\rho$  is the probability of performing no down-sampling.  $c$  controls how sharply the Dirichlet samples cluster and decays with training.  $\varepsilon$  is a small value to prevent zero entries in  $\mathbf{d}$ .  $\pi$  is the training progress factor from 0 to 1.  $\mathbf{d}$  is the progress-weighted blend between an “all-ones” (no downsampling) mix and the target mix  $\mathbf{p}_{\text{tgt}}$ .  $\alpha$  is the Dirichlet *concentration* parameter derived from  $\mathbf{d}$  and  $c$ . Finally,  $\mathbf{p}$  is the vector of per-rate proportions sampled for the current mini-batch. The hyperparameters for the post-training (melt) stage are shown in Table 5.

Table 5: Hyperparameters used in the melt stage.

Symbol	Description	Value
$U$	Maximum downsampling rate	4
$S_p$	Steps to reach target proportions	$10^5$
$\mathbf{p}_{\text{tgt}}$	Target mix over rates $[1, \dots, U]$	$[0.1, 0.45, 0.25, 0.2]$
$c$	Concentration control parameter	30.0
$\varepsilon$	Small constant for stability	$1.0 \times 10^{-6}$
$\rho$	Probability of skipping downsampling	0.5

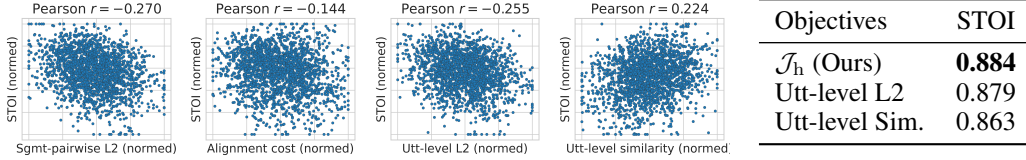


Figure 4: Scatter plots comparing  $\mathcal{J}_h$  with alternative objectives. From left:  $\mathcal{J}_h$ , alignment cost, utterance-level L2 distance and similarity. Each point represents a (downsampling scheme, reconstruction quality) pair. The Pearson coefficient is shown at the top of the picture.

## B Additional results

### B.1 Ablation on different surrogate objectives

We compare our proposed  $\mathcal{J}_h$  (Eq. 4) with several alternative surrogate objectives, including: (1) alignment cost, which measures the match between the downsample segmentation  $\mathbf{s}$  and phone-level alignments computed by Kaldi [48] - this cost penalizes segments that split phone boundaries more heavily than those aligned with phone edges; (2) utterance-level L2 distance between  $\mathbf{h}$  and  $\mathbf{h}'$ ; and (3) utterance-level cosine similarity between  $\mathbf{h}$  and  $\mathbf{h}'$ . To avoid test set contamination, all evaluation samples are selected from LibriSpeech dev-clean, and the DFR foundation model is utilized to reconstruct them, with STOI as the sole metric. We first randomly select 100 utterances, apply 200 random  $2 \times$  downsampling schemes to each. The scatter plots and Pearson coefficients between STOI and objectives are shown in Figure 4 (only 5% of points are plotted for clarity). Results show that alignment cost has the weakest correlation with reconstruction quality. We further evaluate by selecting 200 additional utterances and directly optimizing these three costs in the DP algorithm. As shown in Table 6, schemes optimized for  $\mathcal{J}_h$  also yield superior reconstruction quality.

### B.2 Streaming ability

Although the DP algorithm used in ScheDFR is non-causal, it still supports streaming inference via a chunking strategy. In the chunked streaming mode, the encoder segments the input audio into fixed-length chunks and introduces a small overlap between chunks to mitigate artifacts near chunk boundaries. Additionally, we retain the 3-second left context for each chunk as auxiliary input. Then, the DP-based downsampling scheduler is applied to each chunk feature sequence  $\mathbf{h}$  to obtain the downsampled output  $\mathbf{h}'$  using Algorithm 2. Finally, the decoder receives the quantized feature  $f_Q(\mathbf{h}')$  to reconstruct the waveform, and the outputs of different chunks are stitched together using linear fade-in/fade-out smoothing.

During testing, we still dynamically downsample 80 Hz continuous features to 40 Hz and evaluate on the UniCATS Testset B [43], but in streaming mode under different chunk configurations. The results are summarized in Table 7. When enabling chunking streaming inference, all evaluation metrics exhibit only marginal degradation compared to the non-streaming case, except for SECS, which remains nearly unchanged. As the chunk size increases, WER remains relatively stable while STOI, PESQ, and UTMOS show slight improvements. Increasing the overlap from 25 ms to 50 ms further enhances performance. The best configuration observed is 500 ms chunk size with 50 ms overlap, achieving a WER below 4% and a SECS score even higher than the non-streaming baseline.

Table 7: Streaming inference performance under different chunk sizes and overlaps.

Model	Infernece Frame Rate (Hz)	Chunk Size (ms)	Overlap (ms)	WER (%)↓	STOI↑	SECS↑	MCD↓	UTMOS↑
CodecSlime	40	∞	-	3.82	0.900	0.916	1.83	3.93±0.029
CodecSlime	40	100	25	4.07	0.863	0.903	1.91	2.63±0.032
CodecSlime	40	250	25	4.15	0.884	0.917	1.86	3.31±0.030
CodecSlime	40	500	25	4.16	0.891	0.919	1.85	3.60±0.030
CodecSlime	40	500	50	<b>3.97</b>	<b>0.893</b>	<b>0.919</b>	<b>1.85</b>	<b>3.76±0.031</b>

## C Efforts and analysis on efficiency

### C.1 Inference efficiency

**Vanilla version of the DP downsampling scheduler** Algorithm 2 outlines the vanilla dynamic programming procedure for solving Eq. 3 during inference. The algorithm can be divided into 4 sequential parts. It first pre-computes all segment-wise cohesion losses (Lines 2.2–2.4), then fills the DP table by maximizing cumulative score under the constraint of total target length  $T'$  (Lines 2.5–2.15), and finally recovers the optimal segmentation via back-tracing (Lines 2.16–2.21).

---

**Algorithm 2:** Vanilla version of DP for maximizing  $\mathcal{J}_h$  (Eq. 3)

---

**Input:** Feature  $\mathbf{h} \in \mathbb{R}^{T \times d_m}$ ; target length  $T'$ ; segment upper-bound  $U$

**Output:** Optimal downsampling scheme vector  $\mathbf{s}^*$ ; downsampled features  $\mathbf{h}'$

---

```

1 Step 1: Pre-compute per-segment losses;
2 for  $j \leftarrow 1$  to  $T$  do
3   for  $s \leftarrow 1$  to  $\min(U, j)$  do
4      $L[j][s] = \frac{1}{s} \sum_{a=j}^{j+s-2} \sum_{b=a+1}^{j+s-1} \|h_a - h_b\|_2$ ;

5 Step 2: Initialize DP tables;
6  $d[j][i] \leftarrow -\infty$ ,  $\text{prev}[j][i] \leftarrow 0 \quad \forall 0 \leq j \leq T, 0 \leq i \leq T'$ ;
7  $d[0][0] \leftarrow 0$ ;

8 Step 3: Fill DP;
9 for  $j \leftarrow 1$  to  $T$  do
10   for  $i \leftarrow 1$  to  $\min(j, T')$  do
11     for  $s \leftarrow 1$  to  $\min(U, j - i + 1)$  do
12        $\text{score} \leftarrow d[j - s][i - 1] - L[j][s]$ ;
13       if  $\text{score} > d[j][i]$  then
14          $d[j][i] \leftarrow \text{score}$ ;
15          $\text{prev}[j][i] \leftarrow s$ ;

16 Step 4: Back-trace to obtain  $\mathbf{s}^*$ ;
17  $j \leftarrow T$ ,  $i \leftarrow T'$ ,  $\mathbf{s}^* \leftarrow \langle \rangle$ ;
18 while  $i > 0$  do
19    $s \leftarrow \text{prev}[j][i]$ ;
20   prepend  $s$  to  $\mathbf{s}^*$ ;
21    $j \leftarrow j - s$ ,  $i \leftarrow i - 1$ ;
22  $\mathbf{h}' \leftarrow f_{\text{down}}(\mathbf{h}, \mathbf{s}^*)$ 
23 return  $\mathbf{s}^*$ ,  $\mathbf{h}'$ 

```

---

The two main time-consuming parts are pre-computing (step 1) and DP table filling complexity (step 3), whose total complexity is  $\mathcal{O}(TU^3 + TT'U)$  (here we treat vector add/multiplication as an atomic operation). The efficiency optimization of DP algorithms constitutes a vast and profound research field, encompassing various techniques such as pruning, specialized data structures, and even system-level approaches like polyhedral models [49]. Although in-depth DP optimization is not

the primary focus of this work, we present a simple yet effective trick to prevent model throughput degradation under GPU bottlenecks.

**DP efficiency optimization** Given that DP involves frequent random memory access and logical operations, it demonstrates high efficiency when executed on CPUs. Consequently, by reducing the DP computation time below the backbone processing time (mainly on GPUs) and leveraging CPU-GPU parallelization, we can maintain the overall model throughput.

Table 8: Efficiency comparison of DP algorithm variants.

DP Configuration		Time Measured (s)		
$R_S$	$U$	Backbone	Vanilla DP	Pruned DP
2	4	70.7	86.3	61.2
1.6	4	70.7	92.7	63.1

A simple yet effective pruning strategy involves modifying the loop order in Algorithm 2 (Lines 2.9–2.11) to  $i, s, j$  from outer to inner, where the valid range of  $j$  can be constrained by  $i$  and  $s$ :

$$j \in [\max(i, s, T - (T' - k) \cdot U), \min(T, (i - 1) \cdot U + s, T - (T' - i))] \quad (6)$$

This pruning significantly reduces the number of  $d$  array elements requiring computation and meanwhile keeping the DP results unchanged. For example, for  $U = 4$ ,  $T = 1000$ ,  $T' = 500$  (corresponding to a  $\approx 12$ -second audio input), the required state computations decrease from 2000k to 672k (reduced by 66.4%). Tests on UniCATS Testset B using an NVIDIA A800-SXM4-80GB GPU and Intel Xeon Platinum 8336C CPU @ 2.30GHz (see Table 8) demonstrate that this pruning successfully reduces DP runtime below backbone computation time. Combined with other aforementioned optimizations, the overall DP time efficiency becomes entirely acceptable for practical deployment.

## C.2 Training efficiency

To address the concern on efficiency when integrating downsampling into model training, we apply a fast downsampling procedure (Algorithm 3) that efficiently downsamples speech features. It uses a vectorized implementation, *eliminating explicit loops* while maintaining mathematical equivalence with four key steps. First, it constructs segment indices by repeating and interleaving segment IDs (Line 3.1-2). The core operation employs a `scatter_add` to aggregate features within each segment (Line 3.3-4), followed by element-wise division to compute segment averages (Line 3.5). Finally, a `gather` operation reconstructs the downsampled features (Line 3.6). For batch sizes greater than 1, the features and downsampling schemes can be concatenated along the time axis to form a single batch with batch size 1, enabling efficient unified processing. The `scatter_add` (parallel write with atomic addition) and `gather` (parallel read) operations ensure GPU-friendly memory access patterns, crucial for real-time processing.

---

### Algorithm 3: Fast average downsampling

---

**Input:** input features  $\mathbf{h} \in \mathbb{R}^{T \times D}$ ; max segment length  $U \in \mathbb{N}$ ;

downsample scheme  $\mathbf{s} \in \{1, \dots, U\}^{T'} (\sum_i s_i = T)$

**Output:** downsampled features  $\mathbf{h}' \in \mathbb{R}^{T' \times D}$

---

- 1 `segment_idx`  $\leftarrow [1, \dots, T']$ ;
  - 2 `segment_idx`  $\leftarrow \text{segment\_idx.repeat\_interleave}(\mathbf{s}).\text{repeat}(D, 1)^T \in \mathbb{N}^{T' \times D}$ ;
  - 3 `hsum`  $\leftarrow \mathbf{0} \in \mathbb{R}^{T' \times D}$ ;
  - 4 `hsum`  $\leftarrow \text{h}_{\text{sum}}.\text{scatter\_add}(\text{dim}=0, \text{index}=\text{segment\_idx}, \text{src}=\mathbf{h})$ ;
  - 5 `havg`  $\leftarrow \text{h}_{\text{sum}} \oslash \mathbf{s}.\text{unsqueeze}(1).\text{expand}(T', D)$ ; //  $\oslash$  is element-wise division
  - 6 `h'`  $\leftarrow \text{h}_{\text{avg}}.\text{gather}(\text{dim}=0, \text{index}=\text{segment\_idx}) \in \mathbb{R}^{T' \times D}$ ;
  - 7 **return** `h'`
-

Table 9: Efficiency comparison of fast and slow downsampling algorithms.

Test Configuration				Downsampling Time			Training Time			
Test Size	$T$	$D$	$U$	Fast (ms)	Slow (ms)	Speedup	Backbone (ms)	Fast (ms)	Slow (ms)	Speedup
Small	800	256	4	0.18	15.21	$85.2\times$	-	-	-	-
Medium	1500	512	4	0.18	30.37	$173.2\times$	-	-	-	-
Large	2560	1024	4	0.18	48.98	$276.1\times$	855.9	862.1	933.5	$1.08\times$

As demonstrated in Table 9, the proposed algorithm achieves remarkable speedups across various configurations. In the table, the fast version refers to Algorithm 3, and the slow version is a vanilla downsampling via a for-loop. The “Downsampling Time” part measures the time-consuming for the downsampling process only, whereas the “Training Time” part further tests the total training time (per batch). For large-scale inputs ( $T = 2560, D = 1024$ ), it processes 48.98 ms worth of computation in just 0.18 ms - a  $276\times$  acceleration. The speedup grows with input dimensionality due to better parallelization of the vectorized operations. Notably, when integrated into real model training on an NVIDIA A800-SXM4-80GB GPU (last row), the overhead remains negligible ( $1.01\times$  slowdown vs backbone,  $1.08\times$  speedup vs slow version), confirming its practical viability. These results validate our design’s effectiveness in temporal redundancy compression without compromising pipeline efficiency.

## D Examples

The effectiveness of CodecSlime can be inspected from a few examples. Figure 5 presents three illustrative utterances from the LibriTTS test-clean partition. For each utterance we display, from top to bottom, the waveform, the phone-level alignment obtained with a 12.5 ms frame step (80 Hz), and the optimal down-sample scheme predicted by CodecSlime when the scheduling parameters are  $R_S = 2$  and  $U = 4$ . The alignments are produced by a standard Kaldi forced-alignment recipe [48].

Figure 5 reveals that the optimal segment layout is only partially correlated with the phonetic boundaries. Long pauses or steady vowels are indeed represented by longer segments, showing that the scheduler learns to exploit obvious temporal redundancy. Nevertheless, many segments stretch across phone boundaries, which implies that the best compression strategy for waveform reconstruction cannot be inferred from linguistic segmentation alone; rather, it depends on frame-level acoustic similarity that is difficult to predict a priori. During the *Melt* stage, the model is exposed to a wide variety of merge patterns, which allows it to discover such counter-intuitive yet effective schemes. This observation underscores the necessity of our two-stage training and highlights the advantage of scheduling down-sampling directly from feature space instead of relying on handcrafted heuristics.

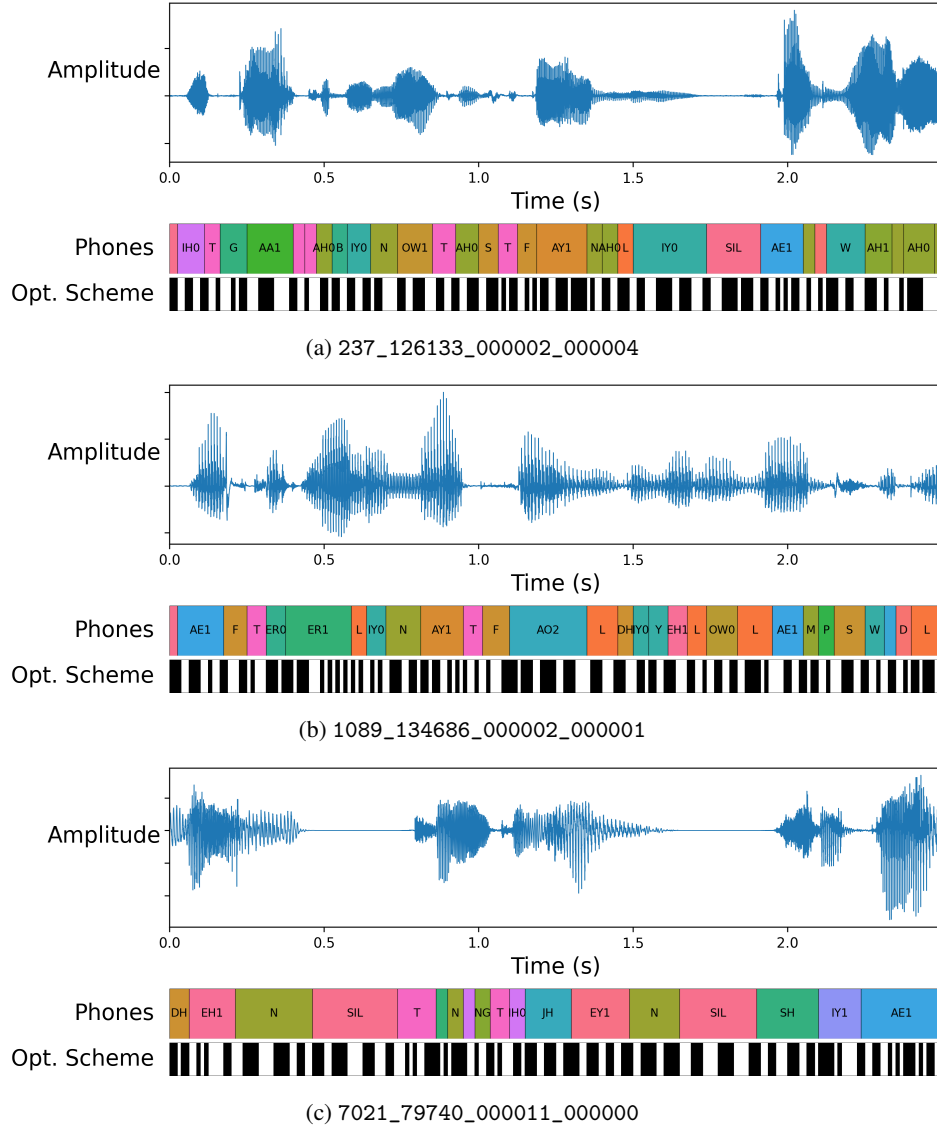


Figure 5: Waveform (top), phone-level alignment (middle), and optimal down-sample scheme (bottom) for three representative utterances. Coloured blocks denote individual phones, while alternating black/white bars show the segment boundaries selected by the dynamic-programming scheduler. All utterances are truncated to 2.5 seconds for clarity.